Structural Studies in Solution of the Recombinant N-Terminal Pair of Short Consensus/Complement Repeat Domains of Complement Receptor Type 2 (CR2/CD21) and Interactions with Its Ligand C3dg[†]

Joel M. Guthridge,[‡] Jonathan K. Rakstang,[‡] Kendra A. Young,[‡] Justin Hinshelwood,[§] Mohammed Aslam,[§] Alexis Robertson,[§] Matthew G. Gipson,[‡] Maria-Rossa Sarrias,[||] William T. Moore,[||] Michael Meagher,[⊥] David Karp,[#] John D. Lambris,[||] Stephen J. Perkins,[§] and V. Michael Holers*[,‡]

Departments of Medicine and Immunology, Division of Rheumatology, University of Colorado Health Sciences Center, Denver, Colorado 80262, Department of Biochemistry and Molecular Biology, Royal Free and University College Medical School, London, U.K., Department of Pathology and Laboratory Medicine, Protein Chemistry Laboratory, University of Pennsylvania, Philadelphia, Pennsylvania 19104, Bioprocess Development Facility, University of Nebraska, Lincoln, Nebraska 68583, and University of Texas Southwestern Medical School, Dallas, Texas 75235

Received January 26, 2001; Revised Manuscript Received March 28, 2001

ABSTRACT: Human complement receptor type 2 (CR2, CD21) is a cell surface receptor that binds three distinct ligands (complement C3d, Epstein−Barr virus gp350/220, and the low-affinity IgE receptor CD23) via the N-terminal two of fifteen or sixteen short consensus/complement repeat (SCR) domains. Here, we report biophysical studies of the CR2 SCR 1-2 domain binding to its ligand C3dg. Two recombinant forms of CR2 containing the SCR 1-2 and SCR 1-15 domains were expressed in high yield in *Pichia pastoris* and baculovirus, respectively. Circular dichroism spectroscopy showed that CR2 SCR 1-2 receptor possessed a β-sheet secondary structure with a melting temperature of 59 °C. Using surface plasmon resonance, kinetic parameters for the binding of either CR2 SCR 1-2 or the full-length SCR 1-15 form of CR2 showed that the affinity of binding to immobilized C3d is comparable for the SCR 1-15 compared to the SCR 1-2 form of CR2. Unexpectedly, both the association and dissociation rates for the SCR 1-15 form were slower than for the SCR 1-2 form. These data show that the SCR 1-2 domains account for the primary C3dg binding site of CR2 and that the additional SCR domains of full-length CR2 influence the ability of CR2 SCR 1-2 to interact with its ligand. Studies of the pH and ionic strength dependence of the interaction between SCR 1-2 and C3d by surface plasmon resonance showed that this is influenced by charged interactions, possibly involving the sole His residue in CR2 SCR 1-2. Sedimentation equilibrium studies of CR2 SCR 1-2 gave molecular weights of 17 000, in good agreement with its sequence-derived molecular weight to show that this was monomeric. Its sedimentation coefficient was determined to be 1.36 S. The complex with C3d gave molecular weights in 50 mM and 200 mM NaCl buffer that agreed closely with its sequence-derived molecular weight of 50 600 and showed that a 1:1 complex had been formed. Molecular graphics views of homology models for the separate CR2 SCR 1 and SCR 2 domains showed that both SCR domains exhibited a distribution of charged groups throughout its surface. The single His residue is located near a long eight-residue linker between the two SCR domains and may influence the linker conformation and the association of C3d and CR2 SCR 1-2 into their complex. Sedimentation modeling showed that the arrangement of the two SCR domains in CR2 SCR 1-2 is highly extended in solution.

Complement receptor type 2 (CR2, CD21)[1] is an integral membrane glycoprotein of size approximately 145 kDa. CR2 is found primarily on mature human B cells and also on follicular dendritic cells, epithelial cells, and some T cells. CR2 plays a critical role in B cell activation and the generation of normal immune responses (*1*−*4*). On the surface of a B cell, CR2 is found in a CR2/CD19/CD81 complex or in a CR2/CR1 complex (*5*, *6*). In the former, the interaction of C3dg-bound antigen with CR2 causes a signal to be transmitted through CD19 to lower the threshold for B cell activation through the B cell receptor. The generation of CR2/CR1 knockout mice has shown that

[†] Supported by Grant R0-1 CA53615 to V.M.H. from the National Institutes of Health, Grant 052615 to S.J.P. from the Wellcome Trust, and National Institutes of Health Grant R0-1 AI30040 and Cancer and Diabetes Centers Core Support Grants CA16520 and DK19525 to J.D.L.

* To whom correspondence should be addressed. E-mail: Michael.Holers@uchsc.edu.

[‡] University of Colorado Health Sciences Center.

[§] Royal Free and University College Medical School.

[||] University of Pennsylvania.

[⊥] University of Nebraska.

[#] University of Texas Southwestern Medical School.

[1] Abbreviations: CR2, complement receptor type 2; SCR, short consensus/complement repeat domain; CR2 SCR 1-2, N-terminal two SCR domains of CR2; CR2 SCR 1-15, SCR domains 1-15 of CR2; IMAC, immobilized metal affinity chromatography; MALDI-TOFMS, matrix-assisted laser desorption ionization−time of flight mass spectroscopy.

10.1021/bi0101749 CCC: $20.00
Published on Web 04/28/2001

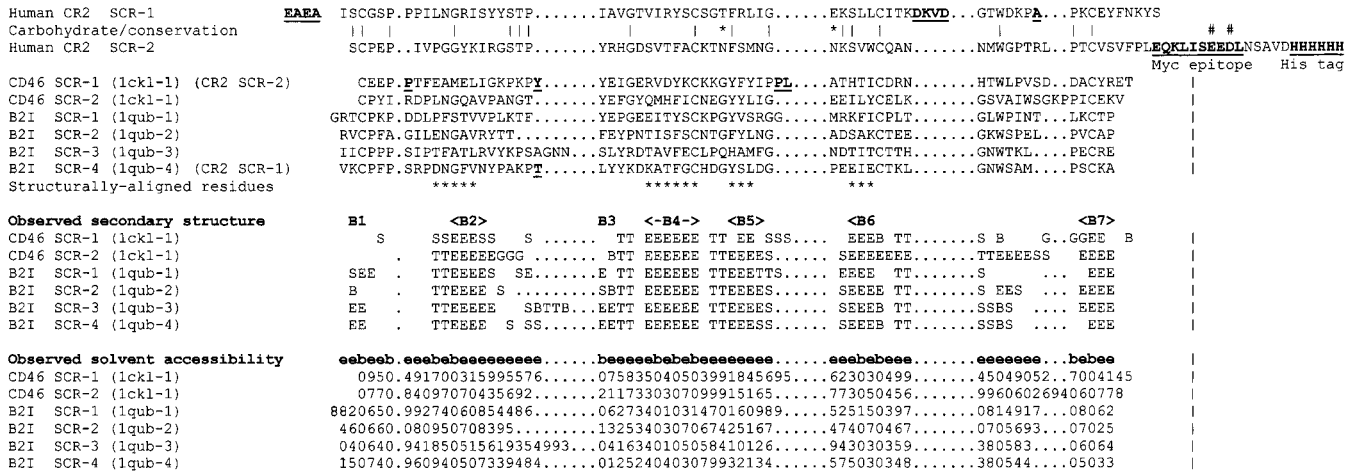

FIGURE 1: Sequence alignment of the first two SCR domains of human CR2 with the crystal structures of the SCR domains. (a) The first two sequences correspond to the predicted sequence of the mature, EndoH-treated, purified CR2 SCR 1-2 protein produced in *P. pastoris* by fermentation. The underlined N-terminal residues EAEA and the C-terminal myc-tag and His-tag residues are vector-derived. The asterisks (*) identify the two potential N-linked glycosylation sites in this protein. The vertical strokes (|) indicate residue conservation. The hatches (#) show the two predicted C-terminal cleavage sites based upon the experimentally determined N-terminal sequence and MALDI-TOFMS mass determinations of the mature protein. (b) The aligned sequences of two SCR domains in CD46 and the first four SCR domains of β2 glycoprotein I are shown, together with the outcome of DSSP analyses of their β-sheet structures (denoted by E: the β-strands are indicated by B1 to B7), and the COMPARER analyses of solvent-accessible residues (e, exposed; b, buried). The two structures used as templates for the modeling of CR2 SCR 1 and SCR 2 are indicated in the left margin. The two insertions and four deletions made during this modeling are shown in bold and underlined.

normal B cell immune responses and germinal center reactions depended upon the appropriate expression and function of the CR2/CR1 molecules on both B cells and follicular dendritic cells (*7*, *8*). Human CR2 also functions as the Epstein−Barr virus (EBV) receptor that mediates infection, activation, and immortalization of human B cells by this virus (*9*−*12*).

CR2 is a member of the regulators of complement activation gene family (*13*). Members of this family contain short consensus/complement repeat (SCR) domains, also known as complement control protein domains. Each SCR domain contains 60−70 amino acid residues, including a conserved disulfide bridge pattern of Cys1→Cys3 and Cys2→Cys4. CR2 contains either 15 or 16 SCR domains followed by a 28 amino acid transmembrane domain and a 34 amino acid cytoplasmic tail. CR2 is unusual in that it binds to at least four distinct ligands. The natural ligand for CR2 is complement component C3d or C3dg, although iC3b will also interact with CR2 (*14*, *15*). The Epstein−Barr virus coat glycoprotein gp350/220 is also a ligand for CR2, in which its binding site overlaps with that for C3d (*16*, *17*). These two ligands bind to the N-terminal pair of SCR domains of CR2 (SCR 1-2) (*14*, *18*). Interferon-α also binds to CR2 (*19*). The low-affinity IgE receptor CD23 binds to CR2 in a carbohydrate-dependent fashion at glycosylation sites in the SCR 5-8 domains and a carbohydrate-independent site within SCR 1-2 (*20*, *21*).

To date, the molecular definition of how CR2 interacts with C3dg and gp350/220 has utilized mutational strategies, the expression of chimeric human/mouse molecules, structurally informative monoclonal antibodies, and linear peptides derived from the receptor or ligand (*15*, *17*, *22*−*27*). Although candidate receptor−ligand interaction sites have been postulated from these studies, these approaches have given inconsistent results. This may result from the three-dimensional characteristics of SCR domains, such as the atypically long eight-residue linker peptide between SCR 1 and SCR 2, in which possible alterations of the relative orientation of these two domains in the different approaches may have affected the identification of the ligand binding site (*25*). Structural studies are accordingly required, and the recent crystal structure of C3d (*28*) represents an important first step in defining the molecular details of its interaction with CR2 SCR 1-2. An appraisal of the structure of full-length CR2 is also required to understand the interaction with C3dg and gp350/220. Hydrodynamic and electron microscopy studies show that this structure is a highly extended and rodlike structure (*29*). However, little is known about the degree of flexibility or the orientations between the SCR domains in the full-length CR2 structure and whether this may influence ligand binding.

In this report, we describe the expression of the CR2 SCR 1-2 domain and have utilized this as well as the CR2 SCR 1-15 domain forms of CR2 to study their interactions with the ligands C3dg and C3d. The structural and ligand binding properties of these two forms of CR2 were analyzed by a combination of surface plasmon resonance and analytical ultracentrifugation. We show from pH and ionic strength studies that these parameters contribute to complex formation, in accordance with earlier data relating to these factors. These and our other results contained herein are discussed in the light of homology models for the CR2 SCR 1 and SCR 2 domains based on recent crystal structures for two SCR proteins (*30*, *31*). We propose extended models for the arrangement of the two SCR domains in CR2 SCR 1-2 in solution.

MATERIALS AND METHODS

(a) Production and Purification of CR2 Recombinant Proteins. The human CR2 SCR 1-2 domain (residues 1−135, SWISSPROT code P20023; Figure 1) was cloned into the expression plasmid pPICZα obtained from InVitrogen, Inc.

(Carlsbad, CA). The expression cassette of the plasmid was multimerized (*32*, *33*), and products from this reaction were again gel purified to allow the selection of dimers, trimers, or higher order multimers. The purified multimers were then religated into the *Bam*HI- and *Bgl*II-digested pPIC-Zα vector. For these studies, a clone that contains a higher order multimer ($n \geq 4$) was constructed to produce the recombinant human CR2 SCR 1-2 domain. This plasmid was designated Jx4.2 and used to transfect the x33 wild-type strain of *Pichia pastoris*. Transfected clones were then selected on yeast extract−peptone−dextrose (YPD) plates to which 100 μg/mL Zeocin was added, and 150 positive clones were individually picked and tested for recombinant protein production.

The initial production of CR2 SCR1-2 using *P. pastoris* was performed by the shake flask method in minimal media (InVitrogen). This was replaced by a fermentation method optimized for higher protein production. In brief, the optimal pH and temperature for protein accumulation was determined by completing a series of fermentations in which the pH was varied between 3.5 and 6.0 and the temperature was varied between 20.0 and 30.0 °C. An inoculation strain consisting of 50 mL of YPD media, followed by another 300 mL of YPD media, was used to amplify a 1 mL frozen stock culture to a final OD_{600} of 4.0−5.0. One hundred fifty milliliters of this starter culture was used to initiate a fermentor culture containing 2 L of *Pichia* basal salt medium (BSM) and 4 mL of PTM1 trace metal salts (*34*) contained within a 7 L (5 L working volume) vessel on a BioFlo III fermentation unit (New Brunswick Scientific Co., Edison, NJ). Dissolved O_2 concentration was maintained at 40%, the temperature at 30 °C, and the pH at 5.0 by using ammonium hydroxide (the sole nitrogen source). When the culture reached approximately 130 g wet cell weight (WCW), 3.0 mL of MeOH was injected into the vessel, and the glycerol feed rate was decreased from 20 to 0 g L^{-1} h^{-1} over a 3 h period. This MeOH injection was used to initiate induction and to ease the transition from growth on glycerol to growth on MeOH. Approximately 2 h after the methanol injection, an exponential feed profile was initiated that would give a targeted specific growth rate (μ) of 0.030 h^{-1}. The methanol was added to the culture according to the equation $F_\theta = (0.84\mu + 0.0071)(X_oV_o)e^{\mu t}$, where F_θ is the methanol feed rate, X_o is the WCW at the start of the feed profile, V_o is the fermentor volume at the start of the feed profile, and t is the fermentation time (*35*). Samples were taken at various time points for determinations of the WCW to monitor the growth conditions of the fermentor culture and for product yield determination. When the WCW reached 400 g/L, which corresponded to an induction time of 60 h, the cell supernatant was collected by centrifugation, immediately frozen in a dry ice ethanol bath, and stored at −80 °C.

To purify CR2 SCR 1-2, the cell supernatant was buffered to pH 4.0 using 10 mM formate, a protease inhibitor cocktail (complete EDTA-free protease tablets, Roche-Boehringer Mannheim) was added, and the supernatant was passed over a SP-Sepharose column (2 × 5 mL SP HiTrap columns) at a flow rate of 4 mL/min at 4 °C. Unbound proteins were washed off, and the bound proteins were eluted using 10 mM formate at pH 4.0 with a 0−0.5 M linear NaCl salt gradient. The eluted CR2 SCR 1-2 material was pooled, concentrated, and deglycosylated overnight at 37 °C with 33 000 units EndoH/mL (NewEngland BioLabs, Beverly, MA). The deglycosylated sample was diluted 1:20 into 10 mM formate, pH 4.0, and passed over SP-Sepharose (2 × 5 mL SP HiTrap columns) at a flow rate of 2 mL/min. Unbound material was washed off the column, and a 0.0−0.5 M NaCl gradient was used to elute the deglycosylated CR2 SCR 1-2. Positive fractions were pooled and concentrated. Some CR2 SCR 1-2 was further purified using a Superdex-75 column in phosphate-buffered saline (PBS: 137 mM NaCl, 2.7 mM KCl, 8.1 mM Na_2HPO_4, 1.5 mM KH_2PO_4, 0.5 mM $MgCl_2$, pH 7.4) to remove small molecular weight contaminants. The protein size and purity was determined by both nonreducing and reducing SDS−PAGE analysis using NuPAGE 10% Bis-Tris gels and MES NuPAGE running buffer (Novex, Inc.). N-terminal amino acid sequencing and matrix-assisted laser desorption ionization−time of flight mass spectroscopy (MALDI-TOFMS) analysis were also performed to confirm the exact molecular mass. For concentration determinations, the absorption coefficient A_{280} (1 cm, 1%) was calculated from the total of Trp, Tyr, and Cys residues in the sequence to be 17.6 (*36*).

Human CR2 SCR 1-15 was expressed in Sf9 insect cells as a recombinant soluble protein in the baculovirus expression system. The cDNA coding for the first 15 SCR domains plus the native human Kozac consensus sequence and signal peptide was cloned into the pVL1393 baculoviral expression vector (Pharmingen, San Diego, CA). A stop codon was introduced prior to the transmembrane domain to create a secreted soluble form of the receptor. After infection of the insect cells with the recombinant baculovirus, ten 500 mL spinner cultures were grown for 5 days at 27 °C. The supernatants were removed, filtered, and concentrated using a 30 000 molecular weight cutoff spiral cartridge (Millipore, Bedford, MA). The concentrate was dialyzed overnight against 10 mM Tris and 10 mM NaCl, pH 8.3. CR2 SCR 1-15 was eluted from a 4 × 20 cm Q-Sepharose anion-exchange column using a 0.01−0.50 M NaCl gradient in loading buffer. Fractions were concentrated using Centricon Plus-80 concentrators and then passed over a 2 × 60 cm Superose-6 gel filtration column. SDS−PAGE pure fractions were pooled and concentrated, and the CR2 SCR 1-15 concentration was determined using the Pierce BCA protein assay with a BSA standard curve.

(b) Production and Purification of C3dg-Biotin and C3d Recombinant Proteins. Human C3dg-biotin was cloned into the pET11b vector (Novagen Inc.). This construct consisted of a bicistronic bacterial expression vector with a T7 promoter, an N-terminal polyhistidine, and a T7 epitope tag, followed by the human C3dg sequence (C3 residues 953−1303, in which Cys1010 at its thioester site was mutated to Ala; SWISSPROT code P01024), a GGGSGGGS linker, and a C-terminal biotinylation signal peptide (BSP, LGGIFEAMKELRD) for *bir*A-catalyzed biotinylation. A second ribosomal binding site allows for translation of the *birA* gene in vivo in cells that also express the recombinant C3dg-BSP protein. This strategy allows for very efficient biotinylation of the recombinant protein in vivo (D. Karp, unpublished data).

C3dg-biotin was produced in the *Escherichia coli* BL21 pLysS Codon Plus strain (Stratagene) transfected with the C3dg bicistronic vector. Ampicillin- and chloramphenicol-resistant colonies were used to start an overnight culture in

minimal media; then these were expanded to 5 L and grown at 37 °C until an OD_{600} of 0.3 was obtained. The cultures were induced with 25 mM IPTG at 28 °C and shaken overnight. The harvested pellets were stored at −70 °C. The pellets were resuspended in PBS at pH 8.0 with complete EDTA-free protease inhibitor tablets (Roche-Boehringer Mannheim) and lysed using four freeze−thaw cycles. DNase (4000 units) and RNase (50 μL of 0.5 mg/mL stock) were added. The lysate was clarified by sonication and centrifugation at 8000*g*; then it was mixed for 30 min with 10 mL of Talon (Co^{2+} IMAC: immobilized metal affinity chromatography) resin. After being packed in a disposable column, unbound material was washed off using PBS at pH 8.0 and 10 mM imidazole, and the C3dg-biotin was eluted by a linear gradient to 100 mM imidazole and further purified using a Superdex-75 gel filtration column. Biotinylation was confirmed by Western blots using strepavidin−horseradish peroxidase, which detected bands that also reacted with a rabbit anti-C3dg antibody.

Human C3d was expressed using a seamless cloning method and the pET15b expression vector (Novagen). The final product was identical to that used to determine its crystal structure (*28*). C3d was produced by transfection of the pET15b-C3d plasmid into BL21 pLysS Codon Plus *E. coli* (Stratagene). Cultures were grown as described for C3dg-biotin above, the bacterial pellet was harvested in DEAE starting buffer (20 mM Tris, pH 7.1) plus complete EDTA-free protease inhibitor tablets, and lysis was performed as described above. C3d was purified using a DEAE HiPrep column, followed by a MonoQ HR5 column in 20 mM Tris, pH 7.1, and a MonoS HR5 column in 50 mM MES, pH 7.0, where in all three cases C3d was eluted using a linear salt gradient up to 1 M NaCl. The protein purity was confirmed using SDS−PAGE, MALDI-TOFMS, N-terminal sequencing, and Western blot analysis using rabbit anti-human C3d polyclonal antibodies (Quidel).

(c) Purification of a 70 kDa Fragment of the EBV gp350/220 Protein. A 70 kDa fragment of the Epstein−Barr virus gp350/220 coat protein (*37*) was cloned into the pVI-Bac transfer vector (Pharmingen, San Diego, CA) (*38*). This contained a melittin signal sequence and a recombinant protein with a C-terminal polyhistidine tag. The 70 kDa fragment of gp350/220 was produced by infecting Sf9 insect cells with the gp350/220-packaged baculovirus particles at an MOI of 3. The cultures were grown, and the culture supernatant was processed as described above for CR2 SCR 1-15. The 70 kDa fragment of gp350/220 was then purified using the Talon IMAC resin as described above for C3dg-biotin. Its N-terminal amino acid sequence was determined to be DPMEAALIV, where DP were added during the cloning. Therefore, the melittin signal sequence is appropriately cleaved, but the native gp350/220 signal sequence is not.

(d) Circular Dichroism Spectroscopy. Circular dichroism spectra were recorded at 20 °C using a Jobin-Yvon CD6 spectropolarimeter with quartz cells of path lengths 0.2 and 0.1 mm. The instrument was calibrated with an aqueous solution of recrystallized d_{10}-camphorsulfonic acid ($\theta^{0.1\%,1cm} = 0.308$ at 290 nm). CR2 SCR 1-2 was dialyzed into 5 mM Tris-HCl and 0.5 mM $MgCl_2$, pH 7.5. Its concentration is required to derive the differential molar extinction coefficient $\Delta\epsilon$, and this was determined to be close to 2 mg/mL from its absorbance at 280 nm (*39*). After subtraction of the buffer spectrum from the CR2 SCR 1-2 spectrum, spectral quantification to obtain the secondary structure content was performed using CONTIN (*40*). The temperature dependence of the molar ellipticity of CR2 SCR 1-2 at 1 mg/mL in 5 mM Tris-HCl, pH 7.5, was determined by following the $\Delta\epsilon$ value at 220 nm while the sample was heated from 25 to 80 °C in 2 °C steps. This temperature dependence was evaluated using the five-parameter sigmoidal regression function of SIGMAPLOT (SPSS Inc., Chicago, IL).

(e) Interaction between CR2 SCR 1-2 and a 70 kDa Fragment of EBV gp350/220 by ELISA. The interaction between CR2 SCR 1-2 and a 70 kDa fragment of EBV gp350/220 was measured using a competition ELISA where 10 μg/mL gp350/220 was used to coat the wells of an ELISA plate. Next, soluble CR2 SCR 1-15 was added in 50 mM phosphate buffer, pH 7.4, and 75 mM NaCl alone or in combination with either CR2 SCR 1-2 or gp350/220 to compete with CR2 SCR 1-15 for interaction with bound gp350/220. The amount of CR2 SCR 1-15 bound to the wells was detected using the monoclonal antibody HB5, which is specific for CR2 SCR 3-4 and does not block ligand interactions (*41*).

(f) Surface Plasmon Resonance. Surface plasmon resonance analysis was performed using a BiaCore 2000 instrument with strepavidin-coupled sensor chips. All analyses were performed in 10 mM HEPES, 50 mM NaCl, 1 mg/mL carboxymethyl-dextran, and 0.05% surfactant P-20, pH 7.4 at 25 °C, in which the NaCl concentration or pH was varied. As different pH or salt concentrations were studied, all buffers were adjusted to minimize the effect on the refractive index due to these buffer changes. The chip regeneration buffer used 1 M NaCl in place of 50 mM NaCl. For kinetic analyses, differing amounts of C3dg-biotin were immobilized onto the sensor chip. Flow cell 1 was left blank, while flow cells 2, 3, and 4 were immobilized with approximately 2000, 1000, and 500 response units (RU) of mass, respectively. The analyte concentrations used a minimum of five values between 500 and 0 nM in a range least influenced by system noise. A flow rate of 30 μL/min was routinely used, with an association phase lasting 150 s and a dissociation phase lasting 300 s. Using BiaEvaluation 3.0 software, kinetic analyses entailed data analyses of a single flow cell after subtraction of the background sensorgram reading. After normalization, the sensorgram data from all analysate concentrations for a single flow cell were analyzed by a global curve-fit algorithm, where the best fit was indicated by low residual and χ^2 values. This analysis yields a association rate k_a, a dissociation rate k_d, and a dissociation constant K_D for the ligand−analyte pair.

(g) Analytical Ultracentrifugation of CR2 SCR 1-2 and C3d. Sedimentation equilibrium experiments of CR2 SCR 1-2 and C3d were performed at 20 °C on a Beckman XLi instrument equipped with an AnTi50 rotor. Runs were acquired in six-sector cells with column heights of 2 mm at rotor speeds of 15 000, 19 000, 23 000, and 27 000 rpm until equilibrium had been reached at each speed after 2 days, as judged by the perfect overlap of consecutive runs measured at 5 h intervals. The sample within the cell was monitored using its absorbance at 280 and 295 nm and by Rayleigh interference optics. For CR2 SCR 1-2, data were obtained using concentrations of 0.5−1.5 mg/mL in PBS, to which

200 mM KCl was added for the control runs. Other CR2 SCR 1-2 data were obtained using concentrations of 1.4, 2.8, and 3.9 mg/mL in 50 mM NaCl and 10 mM HEPES, pH 7.4. Its complex with C3d was measured using concentrations of 0.3, 0.7, and 1.0 mg/mL in 50 and 200 mM NaCl, both in 50 mM HEPES, pH 7.4, after gel filtration on Superdex-200 (Amersham Pharmacia Biotech AB) to remove excess uncomplexed protein. The last three equilibrium curves of each acquisition were analyzed assuming a single association species by the use of Beckman software provided as an add-on to Origin Version 4.1 (Microcal Software Inc., Northampton MA). For this, a partial specific volume of 0.731 mL/g for CR2 SCR 1-2 and 0.746 mL/g for C3d was used (*36*), together with a solvent density of 0.9982 g/mL.

Sedimentation velocity data were acquired over 16 h for CR2 SCR 1-2 at 1.7−5.0 mg/mL in PBS at rotor speeds of 30 000 and 42 000 rpm in two-sector cells with column heights of 12 mm. For the *g(s*)* analyses, successive absorbance and interference scans were recorded at 10 min intervals, the shortest interval possible under standard measurement conditions. In time−derivative analyses, the subtraction of pairs of concentration scans vs radius in the cell eliminates systematic errors from baseline distortions in the cell windows and permits the averaging of many pairs of subtractions. The extrapolation of individual subtractions to the start time gives the *g(s*)* function, which was computed using the DCDT+ program (*42*), from which the sedimentation and diffusion coefficients were determined from the peak position and width, respectively.

(h) Molecular Modeling of CR2 SCR 1-2. In our original study (*25*), the CR2 SCR 1-2 domains were modeled using the NMR structure of the SCR 15 and SCR 16 domains of human complement factor H [PDB code: 1hfh (*43*)]. Here, the CR2 SCR 1-2 sequence was aligned with those of six reference crystal structures in the Protein Data Bank (PDB) database (Figure 1). The identity of an alignment was defined as (the number of identical residues) × 100/(the total number of topologically equivalent positions in the alignment, excluding gaps in either sequence). To assist alignments, secondary structures were identified using DSSP (*44*), residue solvent accessibilities were calculated using a probe of 1.4 Å in the COMPARER program (*45*, *46*), and the superimposed structures were visually inspected using INSIGHT II software (MSI, San Diego) in conjunction with Crystal Eyes stereo glasses. For reason of the higher quality of the coordinates, the SCR modeling was much improved by referencing the first CR2 SCR domain to the fourth SCR domain in the crystal structure of β2 glycoprotein I at 2.7 Å resolution and the second CR2 SCR domain to the first SCR domain in the crystal structure of CD46 at 3.1 Å resolution [PDB codes: 1qub and 1ckl (*30*, *31*)]. These templates involved the least rebuilding of loop structures. CR2 SCR 1 required two loop insertions of one and four residues and the deletion of one residue from loop regions in the template structure (underlined in Figure 1). CR2 SCR 2 required three deletions of one, one, and three residues from loop regions in the template structure (Figure 1). The crystal structure of C3d at 2.0 Å resolution was taken from the Protein Data Bank (*28*) (PDB code: 1c3d).

The rigid body fragment assembly method in HOMOLOGY (MSI, San Diego) was used. Structurally conserved regions were defined from the superimposition of the six crystal structures. For the remodeling of the six loops noted above, a precalculated Cα distance matrix identified loops from the Protein Data Bank that best fitted the corresponding Cα distance matrix calculated from the structurally conserved regions that defined the start and end of each searched loop for a specified number of flanking and intervening residues. Side-chain atoms were automatically generated for both the structurally conserved and variable regions using the template structures and general rules for residue exchanges. The models were refined using energy minimization using DISCOVER (MSI, San Diego), where 300 steps of steepest descent minimization were performed. Each model was assessed using PROCHECK (*47*).

The sedimentation coefficient simulations were based on two-domain or three-domain SCR NMR or crystal structures or the two CR2 SCR homology models which were arranged relative to each other on the basis of separations allowed by the eight-residue linker length. Sphere models were created by placing these coordinates within a three-dimensional array of cubes, each of side length 0.550 nm. Provided that the number of atoms within a given cube exceeded a user-defined cutoff based on the volume of CR2, a sphere of the same volume as the cube (sphere diameter 0.682 nm) was placed at the center of the cube. A hydration of 0.3 g of H_2O/g of glycoprotein and an electrostricted volume 0.0245 nm^3 per bound water molecule was used (*36*) and was modeled using the HYPRO procedure (*48*). Typically about 100 spheres were used in a two-domain model, which increased to about 130 on hydration. Procedures for hydrodynamic simulations based on sphere models have been tested (*49*, *50*). These were used in conjunction with the GENDIA program to calculate the $s^0_{20,w}$ values for the hydrated sphere models.

RESULTS AND DISCUSSION

(a) Production and Characterization of CR2 SCR 1-2. The initial production of CR2 SCR 1-2 employed a *P. pastoris* expression system with shake flasks and minimal media. The recombinant protein production level by this method was 4 mg/L, which was insufficient for structural studies. Accordingly, a fermentation method and its optimization were used to enhance the level of protein production to 80 mg/L. Using the purification described in Materials and Methods, this gave a final yield of 20 mg/L. All physical measurements in this study were performed using protein made by the fermentation method.

SDS−PAGE showed that the CR2 SCR 1-2 product produced by fermentation had a smaller mass than that produced by the shake flask method (Figure 2B). The magnitude of the mass loss corresponded to a loss of both the C-terminal myc-tag and His-tag sequences predicted for this expression system (Figure 1). N-Terminal sequencing of the purified deglycosylated protein revealed a single species. This corresponded to the cleavage of the α-mating factor signal peptide at the Kex2 site to leave the vector residues EAEA... attached to the N-terminus of CR2 SCR 1-2. Since it was suspected that the C-terminal tag peptides had been lost from the fermentation product, the protein was examined by MALDI-TOFMS. Figure 2A indicated a major doublet peak at a mass of 16 046 and 16 236 Da, two other peaks that corresponded to the 2+ and 3+ charged species (apparent masses of 8024 and 5362 Da), and some minor

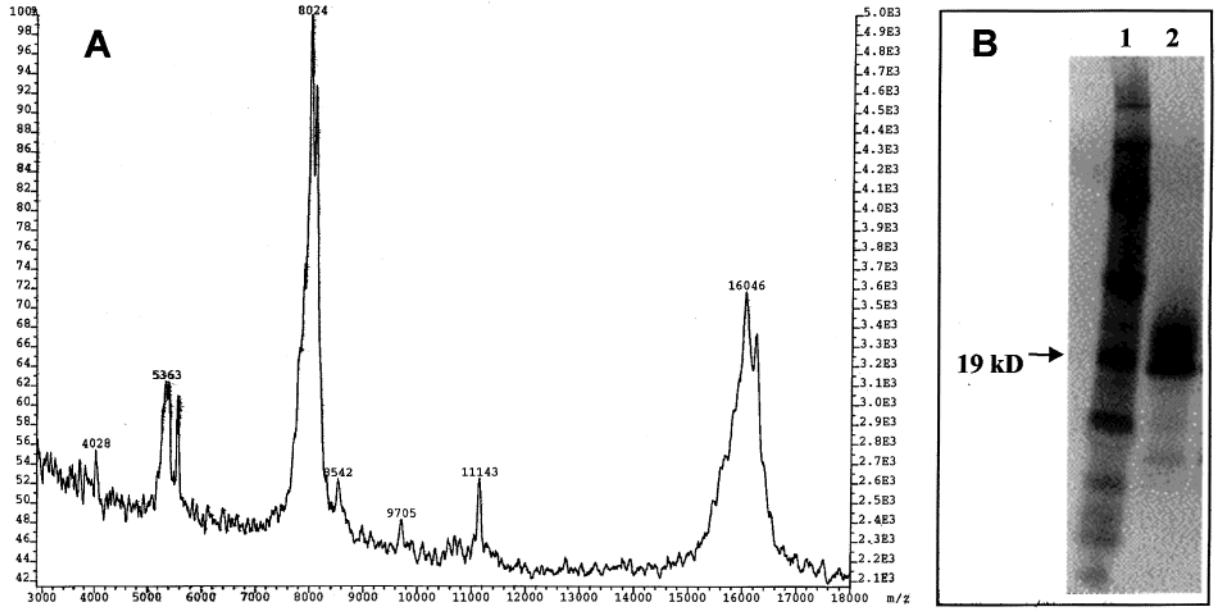

FIGURE 2: Purification of CR2 SCR 1-2 obtained by fermentation. (A) The MALDI-TOFMS spectrum of CR2 SCR 1-2. Molecular masses are indicated as shown. (B) Silver stain of a NuPAGE Bis-Tris MES gel of CR2 SCR 1-2, where lane 1 represents the standards and lane 2 contains 1 μg of CR2 SCR 1-2.

small molecular weight contaminants. The doublet indicated that two major species were present in purified CR2 SCR 1-2, both of which were smaller than the mass of 17 392 Da predicted from the sequence of Figure 1, and is consistent with the outcome of SDS−PAGE. Assuming that two residual GlcNAc residues were present (mass 406 Da), the masses of the doublet in the major peak corresponded to the removal of the C-terminal peptides EEDLNSAVDHHHHHH and DLNSAVDHHHHHH from CR2 SCR 1-2 during fermentation, resulting in predicted CR2 SCR 1-2 masses of 16 002 and 16 260 Da, respectively (Figure 1). Thus, the C-terminus would have lost the polyhistidine sequence and contain a partially cleaved C-terminal *myc*-epitope tag. This would account for the lack of reactivity with the *myc*-epitope as well as the observed inability to purify the recombinant protein on the basis of the polyhistidine tag. On the basis of the mass added by alkylation of CR2 SCR 1-2 with iodoacetamide, MALDI-TOFMS analysis identified a total of eight cysteines in the reduced protein. A separate MALDI-TOFMS analysis showed that no free cysteines were present in the unreduced protein (data not shown). This suggests that all cysteines participated in the formation of the four disulfide bonds predicted for these two domains.

(b) Functional and Structural Assays of Recombinant CR2 SCR 1-2. The ability of recombinant CR2 SCR 1-2 to interact with a plate-bound 70 kDa fragment of EBV gp350/220 was determined using a solution competition ELISA with full-length CR2 SCR 1-15 and an antibody HB5 with biotin attached that was specific for CR2 SCR 3-4 but not for CR2 SCR 1-2 (Figure 3). The decrease in the absorbance at 405 nm showed that the recombinant CR2 SCR 1-2 protein interacted with gp350/220 in the solid phase. In fact, CR2 SCR 1-2 was as effective as soluble gp350/220 in blocking the binding of the CR2 SCR 1-15 form. The use of an irrelevant protein, bovine serum albumin, demonstrated that this competitive effect was specific for the CR2−ligand interaction.

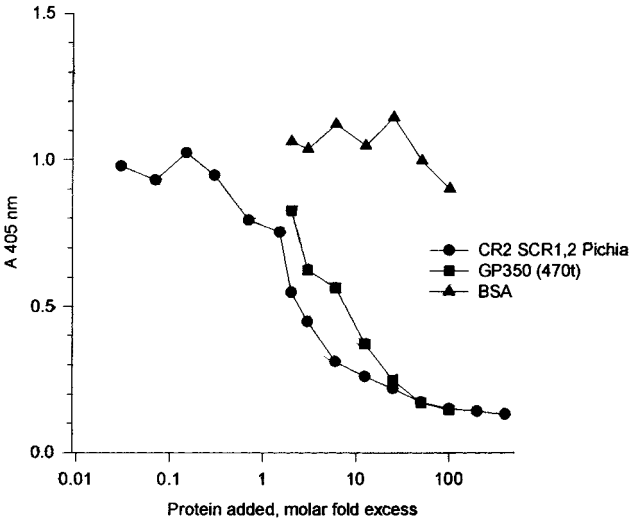

FIGURE 3: Solution competition ELISA where the 70 kDa fragment of gp350/220 was used to coat the solid phase; then the competition between CR2 SCR 1-15 and CR2 SCR 1-2 or that between CR2 SCR 1-15 and gp350/220 was measured. The binding of CR2 SCR 1-15 was followed by the residual binding of the mAb HB5 which will not bind to CR2 SCR 1-2. Bovine serum albumin (BSA) was used as control.

To confirm that recombinant CR2 SCR 1-2 protein was correctly folded, circular dichroism spectroscopy was used in order to monitor its overall secondary structure (*39*). The appearance of the circular dichroic spectrum is consistent with those reported for other SCR-containing β-sheet proteins (Figure 4a) (*51*). Spectral quantification to obtain the secondary structure gave 41−58% β-sheet and 0−10% α-helix, which is as expected. In a second experiment, the temperature dependence of the molar ellipticity at 220 nm of recombinant CR2 SCR 1-2 was followed. This resulted in a sigmoidal curve with a single melting temperature of 59 °C (Figure 4b). There was no suggestion that the two SCR domains had independent melting points. Further evidence for the folding of recombinant CR2 SCR 1-2 was

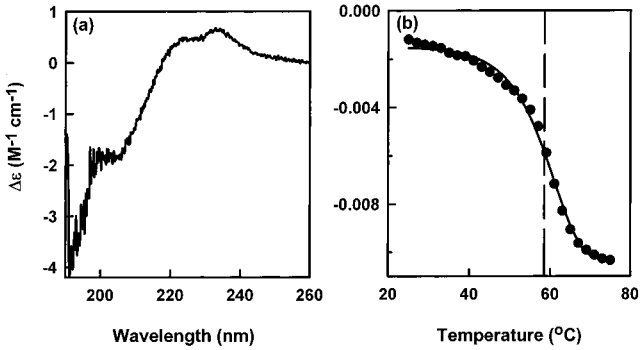

FIGURE 4: Circular dichroism spectroscopy of the CR2 SCR 1-2 sample. (a) The spectrum measured at 1 mg/mL in 5 mM Tris-HCl, pH 7.5 at 20 °C, is shown. (b) In a separate experiment, the temperature dependence of the molar ellipticity at 220 nm under the same conditions used in (a) is shown. The experimental data are represented by filled circles. The five-parameter sigmoidal regression curve fit is represented by the solid line. The midpoint of this curve is denoted by the vertical dashed line and corresponds to a melting temperature of 59 °C.

Table 1: Comparison of Kinetic Parameters for CR2 Binding to C3dg[a]

analyte	k_a ($M^{-1}s^{-1} \times 10^6$)	k_d (s^{-1})	K_D (nM)
CR2 SCR 1-2	9.9 ± 2.5	0.22 ± 0.03	22.4 ± 2.4
CR2 SCR 1-15	2.2 ± 0.2	0.06 ± 0.01	27.1 ± 1.1
	$\rho < 0.05$	$\rho < 0.01$	$\rho > 0.05$

[a] Kinetic values represent the average ± the standard deviation of three experiments. ρ values were determined using an unpaired two-tailed Student's *t*-test analysis.

subsequently obtained from the presence of discrete, well-resolved peaks in HSQC analysis of ^{15}N-labeled protein by 2D NMR spectroscopy (T. Kataleduza, J. Guthridge, T. DeBeer, V. M. Holers, and M. Overduin, data not shown).

(c) Comparison of the Affinities of CR2 SCR 1-2 and CR2 SCR 1-15 for C3dg. Three sets of Biacore surface plasmon resonance studies were performed to quantitatively measure the affinity of the CR2 SCR 1-2 and CR2 SCR 1-15 forms for C3dg. CR2 SCR 1-2 was used in its cleaved form without its His tag. In the first experiments, Biacore studies compared the direct binding of recombinant CR2 SCR 1-2 and CR2 SCR 1-15 to the ligand human C3dg-biotin immobilized to the chip. The differences between panels a and b of Figure 5 indicated that the direct binding curves were different between the two forms of CR2. Global curve fitting of the data demonstrated that the binding model that best described these data is a 1:1 interaction. This showed that the dissociation constants K_D for the CR2 SCR 1-2 and CR2 SCR 1-15 interactions with C3dg were similar at 22.4 ± 2.4 nM and 27.1 ± 1.1 nM, respectively, in 50 mM NaCl, pH 7.4 at 25 °C (Table 1). This difference was not statistically significant. However, CR2 SCR 1-2 both associates and dissociates with C3dg about three to five times faster than CR2 SCR 1-15 as defined by the k_a and k_d, respectively. These data indicated that the required elements in CR2 for C3dg binding were contained within the N-terminal pair of SCR domains, although the larger size of CR2 SCR 1-15 may impede the rate at which binding occurred. The differences in dissociation rates suggest a contribution of the additional SCR domains to the overall affinity of CR2 SCR 1-15 for the ligand C3dg. This may result from either the presence of additional ligand contact

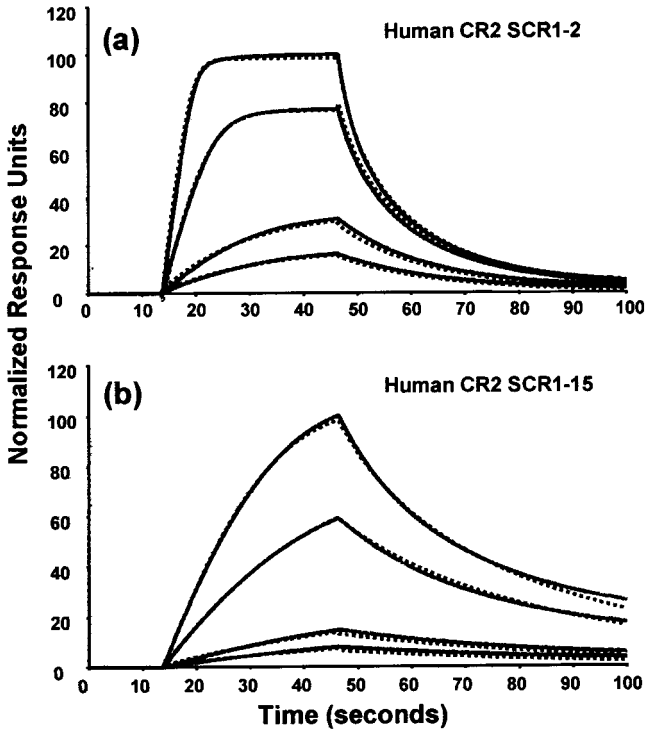

FIGURE 5: Surface plasmon resonance experiments of CR2 SCR 1-2 and CR2 SCR 1-15 binding to the ligand C3dg-biotin. The global curve fits (solid lines) of the normalized sensorgram kinetic data (dashed lines) are shown.

sites somewhere on the SCR 3-15 portion of the CR2 molecule or a cooperativity effect between SCR 1-2 and other SCR domains in CR2. However, the majority of the specificity and strength of interaction of CR2 with the C3dg ligand is localized in the SCR 1-2 domain. Other explanations for this difference were discounted. In terms of the glycosylation of CR2 SCR 1-15 SCR, removal of carbohydrate from CR2 SCR 1-15 did not affect the rate of association with ligand (data not shown). In addition, performing the analysis at multiple flow rates and multiple ligand immobilization levels showed that parameters such as mass transfer effects did not play a role in determining CR2 association rates.

C3d is lacking 47 N-terminal residues found in C3dg (*52*). Since CR2 also interacted with C3d, the affinity of CR2 SCR 1-2 for C3d was also determined in Biacore studies to assess the effect of its smaller size. This experiment also tested whether the additional N- and C-terminal vector-derived residues of C3dg-biotin or its immobilization to the sensor chip had an effect on the interaction with CR2 SCR 1-2. Competition experiments between C3d in solution and C3dg-biotin immobilized to the chip were used to determine an inhibition constant K_I. Figure 6 shows that, as the concentration of C3d increased, a decrease of the maximum sensorgram response was observed. The graph of the percent inhibition versus the concentration of C3d in Figure 6 resulted in the value of K_I at which 50% inhibition was obtained. If the affinity of CR2 SCR 1-2 for C3d is the same as that for C3dg-biotin, the K_I value should be approximately the same as the K_D value (Table 1). The K_I value was determined to be 165 nM, which is approximately a factor of 7−8 greater than the K_D value for the CR2 SCR 1-2−C3dg-biotin interaction at 22.4 ± 2.4 nM but is comparable with it.

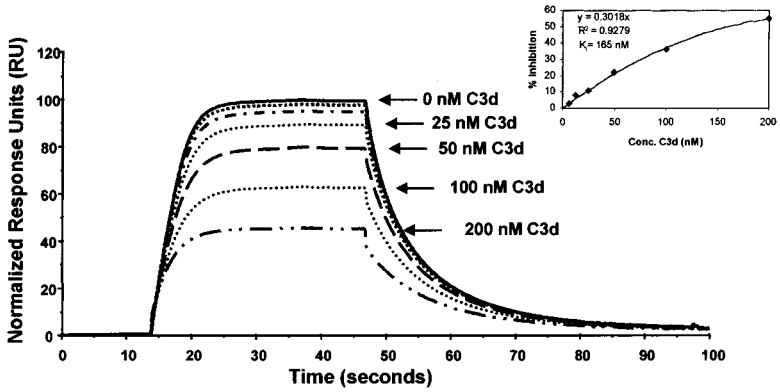

FIGURE 6: Surface plasmon resonance experiments of CR2 SCR 1-2 binding to the ligand C3dg-biotin as a function of the concentration of C3d in the presence of 50 nM CR2 SCR 1-2. The residual CR2 SCR 1-2 binding is shown in the main graph. The comparison of the C3d competitor concentration as a function of the inhibition of analysate binding to the immobilized ligand is shown in the inset. This resulted in the calculation of a K_I value of 165 nM based upon the 50% inhibition point.

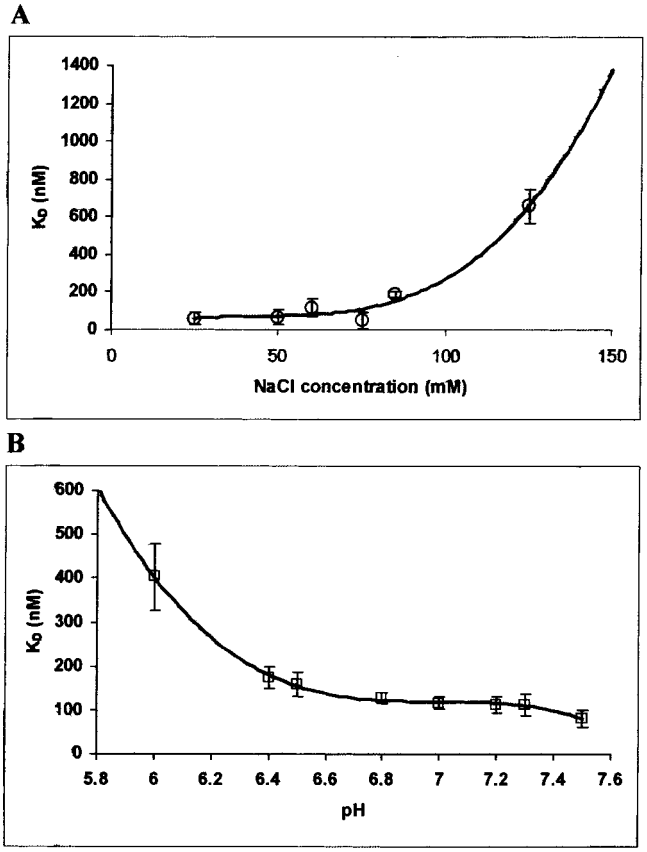

FIGURE 7: Summary of surface plasmon resonance data of the binding of the CR2 SCR 1-2 analyte to the C3dg-biotin coupled ligand. (A) Effect of the ionic strength on the affinity of CR2 SCR 1-2 binding. (B) Effect of pH on the affinity of CR2 SCR 1-2 binding.

A final series of Biacore experiments assessed the effect of ionic strength and pH on the CR2 SCR 1-2−C3dg-biotin interaction. The dependence of the K_D value on the amount of NaCl present showed that an increase in the ionic strength above 100 mM NaCl weakened the receptor−ligand interaction by a factor of 10 (Figure 7A). It is noteworthy that physiological ionic strengths are close to 150 mM NaCl. However, more extensive data in this range of high NaCl concentrations could not be accurately obtained as these conditions were approaching the limits of the Biacore system where the overall noise of the system obscured the ability to reproducibly fit the data and determine K_D. The dependence of the K_D value on the pH is shown in Figure 7B. The affinity is highest at pH 7.4 and is decreased as the pH is lowered. At pH 6.0 and below, the affinity approaches micromolar ranges, at which binding can be observed but the accurate calculation of a K_D value is not possible. This pH dependence implicates the role of a His residue in the formation of the CR2−C3dg complex, in which binding is stronger if the His residue is deprotonated. However, as it is not known if a point of inflection occurs at pH 4 or 5, which would implicate the involvement of a deprotonated Asp or Glu residue in complex formation, this alternative hypothesis cannot be ruled out at present.

(d) Analytical Ultracentrifugation Studies of CR2 SCR 1-2 and Its Complex with C3d. Sedimentation equilibrium measurements by analytical ultracentrifugation were performed to obtain molecular weights. First, CR2 SCR 1-2 produced was studied at concentrations between 0.5 and 1.5 mg/mL in PBS buffer at 20 °C. From the interference data, curve fits based on four different rotor speeds and assuming a single molecular species resulted in a molecular mass of 17 100 ± 1300 Da. This is in good agreement with the expected value of 16 002−16 260 Da (Figure 1). The absorbance data also gave a similar molecular mass of 16 400 ± 1100 Da. Similar results were obtained when 200 mM KCl was added to the buffer. CR2 SCR 1-2 was also studied in HEPES buffer with 50 mM NaCl at concentrations between 1.4 and 3.9 mg/mL in order to replicate the conditions used for surface plasmon resonance. This gave a molecular mass of 16 900 ± 1500 Da, which is in good agreement with the expected molecular weight. These experiments showed that CR2 SCR 1-2 is monomeric in a range of salt concentrations.

The corresponding experiments with the complex between C3d and CR2 SCR 1-2 were performed in the concentration range between 0.3 and 1.0 mg/mL in HEPES buffers containing either 50 mM NaCl or 200 mM NaCl at 20 °C. Data for 50 mM NaCl measured using absorbance and interference optics gave molecular masses of 47 400 ± 2100 and 51 000 ± 1100 Da, respectively, both of which were in good agreement with the sequence-predicted molecular mass of 50 900 Da. Data for 200 mM NaCl measured using absorbance and interference optics gave slightly reduced molecular masses of 42 600 ± 3100 and 47 800 ± 2100 Da, respectively. These agreements showed that the recombinant

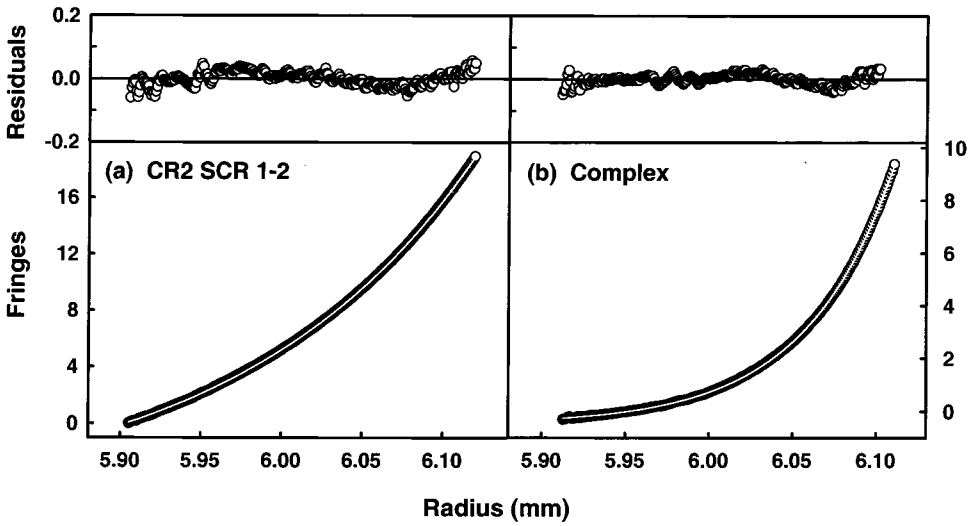

FIGURE 8: Sedimentation equilibrium data for CR2 SCR 1-2 and its complex with C3d. The intensity is shown as a function of radial distribution at equilibrium at a rotor speed of 23 000 rpm for a loading concentration of 3.9 mg/mL for CR2 SCR 1-2 and 1.0 mg/mL for the complex at 20 °C. The data were fitted to a monomer model, which is shown as a line through the experimental data points (○) and resulted in molecular masses of 17 500 and 50 600, respectively, as shown. The corresponding distribution of the residuals in the upper panel (●) is small and random, indicating that a good fit had been obtained.

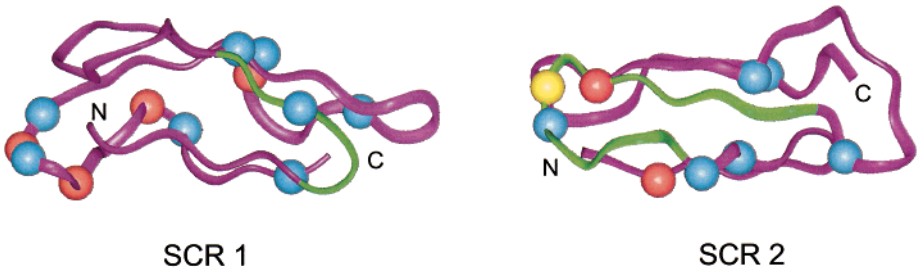

FIGURE 9: Molecular graphics ribbon views of homology models for the CR2 SCR 1 and SCR 2 structures. Basic residues (Lys, Arg) are denoted by blue spheres, and acidic residues (Glu, Asp) are denoted by red spheres. The single His residue is denoted by a yellow sphere. The two CR2 peptides implicated in contacts with C3dg are denoted by green ribbons (residues LNGRIS in SCR 1 and residues GSTPYRHGDSVTFA in SCR 2). On the same scale as shown, the SCR domains are separated by 2.8 nm between the final Cys residue of SCR 1 (denoted by C) and the first Cys residue of SCR 2 (denoted by N), which corresponds to the eight residues between these. This model gives rise to a calculated sedimentation coefficient of 1.36 S.

CR2 SCR 1-2 protein has formed a 1:1 complex with C3d in two salt concentrations that spanned the physiological concentration of 140 mM NaCl.

Sedimentation velocity experiments to determine the sedimentation coefficient were performed at 30 000 and 42 000 rpm using CR2 SCR 1-2 samples at 20 °C and concentrations between 1.7 and 5.0 mg/mL in PBS buffer. Analysis using the *g(s*)* method to analyze pairs of scans showed that the $s_{20,w}$ value was 1.25 ± 0.12 S. The frictional ratio f/f_o was calculated from this to be 1.67 ± 0.15, which is indicative of an elongated domain arrangement within the CR2 SCR 1-2 solution structure.

(e) Molecular Graphics Views of the CR2 SCR 1 and SCR 2 Structures. The effects of pH and ionic strength on the complex formed between CR2 SCR 1-2 and C3d indicated that charged interactions may be important for stabilizing the complex. To determine whether these can be visualized in three-dimensional structures, homology models were created for the separate CR2 SCR 1 and SCR 2 structures using recently determined crystal structures (see Materials and Methods). The sequence alignment showed that a total of six minor insertions and deletions were required to construct homology models from two of the crystal structures. All six occurred in regions other than those of the seven consensus β-strands B1 to B7 that defined the structural core of the SCR domain, and all occurred at positions with high solvent accessibilities (Figure 1). All of the known NMR and crystal structures of the linker residues joining adjacent SCR domains to date correspond to linker lengths of three or four residues between the last Cys residue of the preceding SCR domain and the first Cys residue of the following SCR domain. Their conformations showed much structural variability. As this linker length in CR2 SCR 1-2 is doubled at eight residues, its structure could not be modeled, and this was therefore not done.

The CR2 sequence showed four acidic groups and eight basic groups in SCR 1 and two acidic groups and seven basic groups in SCR 2, with an additional pair of an acidic and a basic residue in the linker. Inspection of the two SCR structures showed that the charged residues were distributed on both sides of each SCR structure (Figure 9). There is some clustering of basic and acidic residues in roughly equal proportions on the upper three-stranded and lower two-stranded surfaces of the SCR domains as viewed in Figure 9. Clusters of basic residues have been shown to be important for function in the SCR 1 and SCR 2 domains in C4b binding protein (*53*, *54*). The two CR2 peptides (LNGRIS and GSTPYRHGDSVTFA) previously identified to be important

for C3d interactions (*25*) both possess an Arg residue. The second peptide also possesses the only His residue in the SCR CR2 1-2 sequence at position 90 as well as an Asp residue. As a His residue may be implicated in complex formation from the Biacore analyses, this is consistent with the involvement of the second peptide in the CR2−C3d complex. This second sequence encompasses a complete loop at one end of the SCR 2 domain that is adjacent to the linker sequence between SCR 1 and SCR 2. This loop is at the opposite end of the structure from the two carbohydrate sites in CR2 SCR 1-2, at which the carbohydrate chains may offer steric hindrance to complex formation with C3d, and so is unlikely to form a C3d binding site (Figure 9). While no molecular details of a C3dg binding site can be deduced from these CR2 SCR models, the models nonetheless offer a possible explanation of the observed ionic and pH effects in complex formation in terms of a His residue at the center of the CR2 SCR 1-2 structure.

Molecular modeling calculations were performed with arrangements of possible CR2 SCR 1-2 structures that were permitted by the eight-residue linker between SCR 1 and SCR 2. This assessed whether these two CR2 domains were extended far apart from each other in a dumbbell-shaped structure or in a compact U-shaped folded-back structure. The sedimentation coefficient of the SCR 15-17 domains of complement receptor type 1 is 1.89 S (*51*). A trial calculation based on the three-domain arrangement of SCR 1-3 seen in the crystal structure of β2 glycoprotein I gave 1.92 S, which agrees well with this experimental value. The sedimentation coefficient of the SCR 2-3 domains of vaccinia virus complement control protein is 1.44 S (*55*). Trial calculations based on six two-domain arrangements of SCR domains seen in four NMR and crystal structures gave a mean value of 1.64 ± 0.05 S that was also comparable with the experimental value. These calculations showed that the usual assumption of extended SCR arrangements replicated the experimental sedimentation coefficients. The same calculation for a CR2 model in which the linker between the two SCR domains was maximally extended (Figure 9) gave a value of 1.36 S, and that for a U-shaped compact folded-back arrangement gave 1.66 S. In comparison with the experimental value of 1.25 ± 0.12 S, the calculations favor an extended arrangement for the two SCR domains of CR2 in solution. While the N-terminal and C-terminal unordered peptides could not be modeled for these comparisons, it was assumed that their effect on these calculations can be discounted.

CONCLUSIONS

To obtain important information concerning the physical and functional characteristics of human CR2, this study has described the successful production by a fermentation approach of the smallest form of this protein that is capable of binding ligands such as C3dg and a 70 kDa fragment of Epstein−Barr virus gp350/220 protein. Previously, the N-terminal pair of SCR domains in CR2 was defined to be the ligand-interacting domains (*14*, *17*, *18*, *29*). In these studies, the expression systems and the resulting protein production levels precluded the present structural studies to define the interaction between CR2 SCR 1-2 and C3d. Here, by the use of a *P. pastoris* expression system, it is possible to produce a properly folded and functionally active form of CR2 SCR 1-2 at levels approaching 80 mg/L before purification. The use of N-terminal sequencing, MALDI-TOFMS, and circular dichroism showed that CR2 SCR 1-2 had been expressed as desired. This enabled us to perform surface plasmon resonance and ultracentrifugation studies.

Our recombinant CR2 SCR 1-2 protein is functionally active. This was demonstrated by solid-state ELISA-based assays and surface plasmon resonance assays in which CR2 SCR 1-2 interacted effectively with two of the ligands for human CR2, a 70 kDa fragment of EBV gp350/220, and C3dg. Earlier studies of the interaction of human CR2 with its ligands had not directly compared the affinity of CR2 SCR 1-2 with that of the soluble full-length form CR2 SCR 1-15 (*14*, *17*, *18*, *29*). The present studies are the first to directly compare the kinetic parameters of these two forms of CR2 with the ligands C3dg and C3d. Surface plasmon resonance showed that the overall ligand affinity of CR2 SCR 1-2 is similar to that of CR2 SCR 1-15. It was concluded that most of the structural information required for the interaction of CR2 with these ligands is contained within the first two domains. However, there is some contribution of the additional SCR domains of CR2 in ligand binding because it was also observed that the rate of association of CR2 SCR 1-2 and 1-15 with its ligand differed, in that CR2 SCR 1-2 interacted with C3dg more rapidly than CR2 SCR 1-15. The simplest explanation for this is that CR2 SCR 1-15 adopts a solution conformation of SCR domains that sterically partly precludes its direct binding to ligand. Only a fraction of the CR2 SCR domains of the receptor may be in an appropriate conformation to interact with ligand at any one time. In addition, it was observed that CR2 SCR 1-2 dissociated from C3dg faster than CR2 SCR 1-15. It is possible that the solution conformation of other SCR domains in CR2 SCR 1-15 may sterically retard the dissociation of C3dg when this is compared to CR2 SCR 1-2. In addition, there may be additional weak sites for C3dg that are present in the SCR domains 3-15 of CR2 that may account for the difference in the dissociation rate constant.

Our examination of the effects of ionic strength and pH upon the affinity of the interaction between CR2 SCR 1-2 and C3dg suggests that the single His residue in CR2 SCR 1-2 may be implicated in this receptor−ligand interaction. This conclusion is consistent with the conservation of this residue in both human and mouse CR2 and with the identification of the SCR 2 peptide GSTPYRHGDSVTFA as a C3d contact site, but it is not unambiguous as C3d itself has four His residues. In addition, as pointed out above, we cannot yet rule out the involvement of Asp or Glu residues. Our results extend previous studies that also concluded that high salt concentration and pH affected the affinity of the interaction (*27*, *29*, *53*, *54*). In these studies, it should be noted that, even at physiological salt concentrations or pH values at or below 6.0, the receptor−ligand interaction could be detected by surface plasmon resonance and analytical ultracentrifugation. Thus, even though the affinities of CR2 SCR 1-2−C3dg interactions at physiological salt or low pH were in the micromolar range or higher, the interaction does occur under those conditions.

Molecular modeling studies of the structure of CR2 SCR 1-2 offered explanations for the ultracentrifugation structural data. This protein possesses one of the longest linker peptides seen between adjacent SCR domains in the complement

proteins. Test calculations based on known linker structures show good agreements between extended SCR structures and the experimental sedimentation coefficient. On that basis, the experimental sedimentation coefficient value for this protein is low compared to other values and indicates that this linker peptide in free CR2 SCR 1-2 is extended. Flexibility in the conformation of this peptide will therefore be an important consideration when providing a molecular explanation of the functional properties of the intact CR2 SCR 1-15 protein.

ACKNOWLEDGMENT

We thank Dr. J. Cambier for the use of his Biacore 2000 instrument, Mr. B. Plantz for assistance with the fermentation, Ms. Y. Harrison-Shahan for protein sequencing, and Mr. Jayesh Gor and Miss Anne-Sophie Perrin for excellent technical support with the analytical ultracentrifuge.

REFERENCES

1. Ahearn, J. M., and Fearon, D. T. (1989) *Adv. Immunol. 46*, 183−219.
2. Pepys, M. B. (1974) *J. Exp. Med. 140*, 126−145.
3. Dempsey, P., Allison, M., Akkaraju, S., Goodnow, C., and Fearon, D. (1996) *Science 271*, 348−350.
4. Carroll, M. C., and Fischer, M. B. (1997) *Curr. Opin. Immunol. 9*, 64−69.
5. Tedder, T. F., Zhou, L.-J., and Engel, P. (1994) *Immunol. Today 15*, 437−442.
6. Carter, R. H., and Fearon, D. T. (1992) *Science 256*, 105−107.
7. Ahearn, J. M., Fischer, M. B., Croix, D. A., Georg, S., Ma, M., Xia, J., Zhou, X., Howard, R. G., Rothstein, T. L., and Carroll, M. C. (1996) *Immunity 4*, 251−262.
8. Molina, H., Holers, V. M., Li, B., Fang, Y.-F., Mariathasan, S., Goellner, J., Strauss-Schoenberger, J., Karr, W. R., and Chaplin, D. D. (1996) *Proc. Natl. Acad. Sci. U.S.A. 93*, 3357−3361.
9. Weis, J. J., Tedder, T. F., and Fearon, D. T. (1984) *Proc. Natl. Acad. Sci. U.S.A. 81*, 881−885.
10. Nemerow, G. R., Wolfert, R., McNaughton, M. E., and Cooper, N. R. (1985) *J. Virol. 55*, 347−351.
11. Ahearn, J. M., Hayward, S. D., Hickey, J. C., and Fearon, D. T. (1988) *Proc. Natl. Acad. Sci. U.S.A. 85*, 9307−9311.
12. Carel, J.-C., Frazier, B., Ley, T. J., and Holers, V. M. (1989) *J. Immunol. 143*, 923−930.
13. Hourcade, D., Holers, V. M., and Atkinson, J. P. (1989) *Adv. Immunol. 45*, 381−416.
14. Lowell, C. A., Klickstein, L. B., Carter, R. H., Mitchell, J. A., Fearon, D. T., and Ahearn, J. M. (1989) *J. Exp. Med. 170*, 1931−1946.
15. Molina, H., Kinoshita, T., Webster, C. B., and Holers, V. M. (1994) *J. Immunol. 153*, 789−795.
16. Nemerow, G. R., Houghten, R. A., Moore, M. D., and Cooper, N. R. (1989) *Cell 56*, 369−377.
17. Martin, D. R., Yuryev, A., Kalli, K. R., Fearon, D. T., and Ahearn, J. M. (1991) *J. Exp. Med. 174*, 1299−1311.
18. Carel, J.-C., Myones, B. L., Frazier, B., and Holers, V. M. (1990) *J. Biol. Chem. 265*, 12293−12299.
19. Delcayre, A. X., Salas, F., Mathur, S., Kovats, K., Lotz, M., and Lernhardt, W. (1991) *EMBO J. 10*, 919−926.
20. Aubry, J. P., Pochon, S., Graber, P., Jansen, K. U., and Bonnefoy, J. Y. (1992) *Nature 358*, 505−507.
21. Aubry, J. P., Pochon, S., Gauchat, J. F., Nueda-Marin, A., Holers, V. M., Graber, P., Siegfried, C., and Bonnefoy, J. Y. (1994) *J. Immunol. 152*, 5806−5813.
22. Nemerow, G. R., Wolfert, R., McNaughton, M. E., and Cooper, N. R. (1985) *J. Virol. 55*, 347−351.
23. Martin, D. R., Marlowe, R. L., and Ahearn, J. M. (1994) *J. Virol. 68*, 4716−4726.
24. Molina, H., Brenner, C., Jacobi, S., Gorka, J., Carel, J.-C., Kinoshita, T., and Holers, V. M. (1991) *J. Biol. Chem. 266*, 12173−12179.
25. Molina, H., Perkins, S. J., Guthridge, J., Gorka, J., Kinoshita, T., and Holers, V. M. (1995) *J. Immunol. 154*, 5426−5435.
26. Rao, P. E., Wright, S. D., Westberg, E. F., and Goldstein, G. (1985) *Cell. Immunol. 93*, 549−555.
27. Clemenza, L., and Isenman, D. E. (2000) *J. Immunol. 165*, 3839−3848.
28. Nagar B., Jones, R. G., Diefenbach, R. J., Isenman, D. E., and Rini, J. M. (1998) *Science 280*, 1277−1281.
29. Moore, M. D., DiScipio, R. G., Cooper, N. R., and Nemerow, G. R. (1989) *J. Biol. Chem. 264*, 20576−20582.
30. Bouma, B., de Groot, P. G., van den Elsen, J. M. H., Ravelli, R. B. G., Schouten, A., Smmelink, M. J. A., Derksen, R. H. W. M., Kroon, J., and Gros, P. (1999) *EMBO J. 18*, 5166−5174.
31. Casanovas, J. M., Larvie, M., and Stehle, T. (1999) *EMBO J. 18*, 2911−2922.
32. Cohen, B., and Carmichael, G. G. (1986) *DNA 5*, 339−343.
33. Takeshita, S., Kezuka, K.-I., Takahashi, M., Honkawa, H., Matsuo, A., Matsuishi, T., and Hashimoto-Goto, T. (1988) *Gene 71*, 9−18.
34. Stratton, J., Chiruvolu, V.-J., and Meagher, M. (1998) in *Pichia Protocols* (Higgens, D. R., and Cregg, J. M., Eds.) pp 107−120, Humana Press, Totowa, NJ.
35. Zhang, W., Bevins, M. A., Plantz, B. A., Smith, L. A., and Meagher, M. M. (2000) *Biotechnol. Bioeng. 70*, 1−8.
36. Perkins, S. J. (1986) *Eur. J. Biochem. 157*, 169−180.
37. Hedrick, J. A., Lao, Z., Wang, Y., Todd, S. C., Lambris, J. D., and Tsoukas, C. D. (1994) *J. Immunol. 153*, 4418−4426.
38. Tessier, D. C., Thomas, D. Y., Khouri, H. E., Laliberte, F., and Vernet, T. (1991) *Gene 98*, 177−183.
39. Drake, A. F. (1994) in *Methods in Molecular Biology* (Jones, C., Mulloy, B., and Thomas, A. H., Eds.) pp 219−244, Humana Press, Totowa, NJ.
40. Provencher, S. W. (1982) *Comput. Phys. Commun. 27*, 213−242.
41. Tedder, T. F., Clement, L. T., and Cooper, M. D. (1984) *J. Immunol. 133*, 678−683.
42. Philo, J. (2000) *Anal. Biochem. 279*, 151−163.
43. Barlow, P. N., Steinkasserer, A., Norman, D. J., Kieffer, B., Wiles, A. P., Sim, R. B., and Campbell, I. D. (1993) *J. Mol. Biol. 232*, 268−284.
44. Kabsch, W., and Sander, C. (1983) *Biopolymers 22*, 2577−2637.
45. Lee, B., and Richards, F. M. (1971) *J. Mol. Biol. 55*, 379−400.
46. Sali, A., and Blundell, T. L. (1990) *J. Mol. Biol. 212*, 403−428.
47. Laskowski, R. A., MacArthur, M. W., Moss, D. S., and Thornton, J. M. (1993) *J. Appl. Crystallogr. 26*, 283−291.
48. Ashton, A. W., Boehm, M. K., Gallimore, J. R., Pepys, M. B., and Perkins, S. J. (1997) *J. Mol. Biol. 272*, 408−422.
49. Smith, K. F., Harrison, R. A., and Perkins, S. J. (1990) *Biochem. J. 267*, 203-212.
50. Perkins, S. J., Smith, K. F., Kilpatrick, J. M., Volanakis, J. E., and Sim, R. B. (1993) *Biochem. J. 295*, 87−99.
51. Kirkitadze, M. D., Krych, M., Uhrin, D., Dryden, D. T. F., Smith, B. O., Cooper, A., Wang, X., Hauhart, R., Atkinson, J. P., and Barlow, P. N. (1999) *Biochemistry 38*, 7019−7031.
52. de Bruijn, M. H. L., and Fey, G. H. (1985) *Proc. Natl. Acad. Sci. U.S.A. 82*, 708−712.
53. Blom, A. M., Berggard, K., Webb, J. H., Lindahal, G., Villoutreix, B. O., and Dahlback, B. (2000) *J. Immunol. 164*, 5328−5336.
54. Blom, A. M., Webb, J., Villoutreix, B. O., and Dahlback, B. (1999) *J. Biol. Chem. 274*, 19237−19245.
55. Kirkitadze, M. D., Henderson, C., Price, N. C., Kelly, S. M., Mullin, N. P., Parkinson, J., Dryden, D. T. F., and Barlow, P. N. (1999) *Biochem. J. 344*, 167−175.

BI0101749